Hirata and Ohta *Earth, Planets and Space* (2016) 68:203
DOI 10.1186/s40623-016-0578-y

Earth, Planets and Space

LETTER

Open Access

Spatial and temporal characteristics of optimum process noise values of tropospheric parameters for kinematic analysis of Global Navigation Satellite System (GNSS) sites in Japan

Yu'ichiro Hirata and Yusaku Ohta*

Abstract

Kinematic analysis of Global Navigation Satellite System (GNSS) data is useful for the extraction of crustal deformation phenomena occurring over short timescales ranging from seconds to 1 day, such as coseismic and postseismic deformation following large earthquakes. However, a fundamental challenge in kinematic GNSS analysis is to separate unknown parameters, such as site coordinate and tropospheric parameters, due to the strong correlation between them. In this study, we assessed the spatial and temporal characteristics of process noise for unknown tropospheric parameters such as zenith wet tropospheric delay and tropospheric gradient by means of kinematic precise point positioning analysis using Kalman filtering across the Japanese nationwide continuous GNSS network. We estimated kinematic site coordinate time series under different process noise combinations of zenith wet tropospheric delay and tropospheric gradient. The spatial distribution of the optimum process noise value for the zenith wet tropospheric parameter with vertical site coordinate time series clearly showed regional characteristics. In comparison with the wet tropospheric parameter, the spatial characteristics of the tropospheric gradient parameter are less well defined within the scale of the GNSS network. The temporal characteristics of the optimum process noise parameters for each site coordinate component at specific sites indicated a clear annual pattern in the tropospheric gradient parameter for the horizontal components. Finally, we assessed the effects on the kinematic GNSS site coordinate time series of optimizing tropospheric parameter process noise. Compared with recommended process noise values from previous studies, the use of estimated "common" optimum process noise values improved the standard deviation of coordinate time series for the majority of stations. These results clearly indicate that the use of appropriate process noise values is important for kinematic GNSS analysis.

Keywords: GNSS, Process noise, Annual signal, Kinematic GNSS analysis, Kalman filtering

Introduction

The application of a Global Navigation Satellite System (GNSS) to the understanding of crustal deformation has significant advantages. Kinematic analysis of GNSS data is a key technique for understanding short-timescale crustal deformation with periods of less than 1 day and has been utilized in many studies of crustal deformation. In particular, high sampling rate (e.g., interval of 1 Hz or greater) kinematic GNSS analysis can be used to detect seismic waves caused by large earthquakes. Larson et al. (2003) found good agreement between surface displacements integrated from strong ground-motion records and long-baseline (several 100 km) 1-Hz GNSS position estimates for the 2002 Denali earthquake. Other studies have similarly succeeded in detecting seismic waves caused by

*Correspondence: yusaku.ohta.d2@tohoku.ac.jp
Research Center for Prediction of Earthquakes and Volcanic Eruptions, Graduate School of Science, Tohoku University, 6-6 Aza-Aoba, Aramaki, Aoba-ku, Sendai 980-8578, Japan

large earthquakes (e.g., Ohta et al. 2006; Bilich et al. 2008). Furthermore, several studies deduced the rupture processes of large earthquakes from high sampling rate kinematic GNSS time series (e.g., Miyazaki et al. 2004; Yokota et al. 2009; Delouis et al. 2010). Recently, kinematic GNSS analysis has been used for real-time estimation of the magnitude and fault expansion of large earthquakes (e.g., Ohta et al. 2012, 2015; Melgar et al. 2013, 2015; Melgar and Bock 2013; Kawamoto et al. 2016).

These previous studies mainly focused on the coseismic time period. Miyazaki and Larson (2008) subsequently investigated early after slip following the 2003 Tokachi-oki earthquake, deduced from 30-s baseline kinematic GNSS analysis, in which they assumed a tightly constrained random walk stochastic process for coordinate estimation (Larson and Miyazaki 2008). Kinematic GNSS time series usually show large disturbances in the lower frequency band (e.g., Genrich and Bock 2006), due to the difficulty of strict separation between the coordinate parameters and other unknown parameters, such as the tropospheric parameters.

The tropospheric delay (TD) provides information on the amount of water vapor integrated over the path between a GNSS satellite and a receiver. TD is a function of zenith distance or satellite elevation (e.g., Davis et al. 1985) and is factorized into dry (hydrostatic) and wet components. In precise GNSS data processing, the zenith total delay (ZTD) is typically estimated as a function of time. Approximately 90% of the total TD caused by refraction is due to the hydrostatic tropospheric component. The hydrostatic component strongly depends on atmospheric pressure at the Earth's surface; thus, it can be accurately modeled. The remaining 10% of the total TD comprises the wet tropospheric component, which is spatially and temporally dependent on the water vapor in the atmosphere and is therefore much more difficult to model precisely (e.g., Webb et al. 2016). Furthermore, the tropospheric delay gradient model (e.g., MacMillan 1995) expresses the tropospheric delay as a combination of the ZTD and an additional term to express azimuthal dependence, represented by the tropospheric delay gradient. Bar-Sever et al. (1998) investigated the impact of tropospheric delay gradient estimates in precise GPS analysis, using GIPSY-OASIS software (Lichten and Border 1987). GIPSY-OASIS adopts a Kalman filter-based (KF) approach, which is useful for estimating the unknown time-dependent parameters. The standard least squares method is typical and robust in estimating daily GNSS coordinates, but is unsuitable for more frequent coordinates and for simultaneously estimating a large number of unknown parameters. In KF-based processing, we must assume the stochastic process mode, such as white noise or random walk, for each unknown parameter. Furthermore, we also must assume process noise values for each time-dependent unknown parameter. These process noise values control the dynamics of the unknown parameters. However, setting these parameters, including each process noise value, is strongly dependent on the method of analysis. In a study by Bar-Sever et al. (1998), the optimum strategy comprised a low-elevation cutoff angle (7°), combined with a model of the zenith wet delay (ZWD) and tropospheric gradient as a relatively low random walk process noise value (5×10^{-8} km $s^{-1/2}$ for ZWD and 5×10^{-9} km $s^{-1/2}$ for tropospheric gradient, respectively). These optimum tropospheric parameters have now been adopted as one of the recommended values in GIPSY-OASIS for kinematic coordinate estimation in a slow-moving body. The process noise values for tropospheric parameters usually adopt units of "mm $h^{-1/2}$." In this study, however, we adopted units of "km $s^{-1/2}$" because this is used in GIPSY-OASIS for setting the process noise of tropospheric parameters. Penna et al. (2015) showed that kinematic precise point positioning (PPP) with appropriately tuned process noise constraints is capable of recovering synthetic tidal displacements. They searched for optimum process noise for the ZWD and coordinate time series based on long-term GNSS data from each site and concluded that tuned coordinate and ZWD process noise values enable accurate 0- to 6-mm amplitude semi-diurnal and diurnal periodic tidal ground displacements to be detected with accuracy better than 0.2 mm. Those results clearly indicate the importance of determining the optimum process noise of unknown parameters under a stochastic process approach for precise GNSS data analysis. In particular, the treatment of process noise is fundamentally important for kinematic analysis because the coordinate time series must be solved using limited data compared to static analysis.

Based on these background studies, we assess the spatial and temporal characteristics of the optimum process noise settings of unknown tropospheric parameters for kinematic PPP data analysis. In this paper, we initially focus on the spatial distribution of the optimum parameter settings between ZWD and tropospheric gradient across the Japanese nationwide GNSS network, which comprises more than 1300 stations. We also discuss the long-term stability of the optimum tropospheric parameters for specific sites. Finally, we discuss the effects of optimizing process noise for kinematic GNSS data analysis.

GNSS data and analysis

We used data from GEONET, which is a dense nationwide GNSS network established by the Geospatial Information Authority of Japan (GSI) comprising more than 1300 stations, to assess the spatial and temporal dependency of the optimum process noise values. Thirty-second dual-frequency phase data were used for processing. This

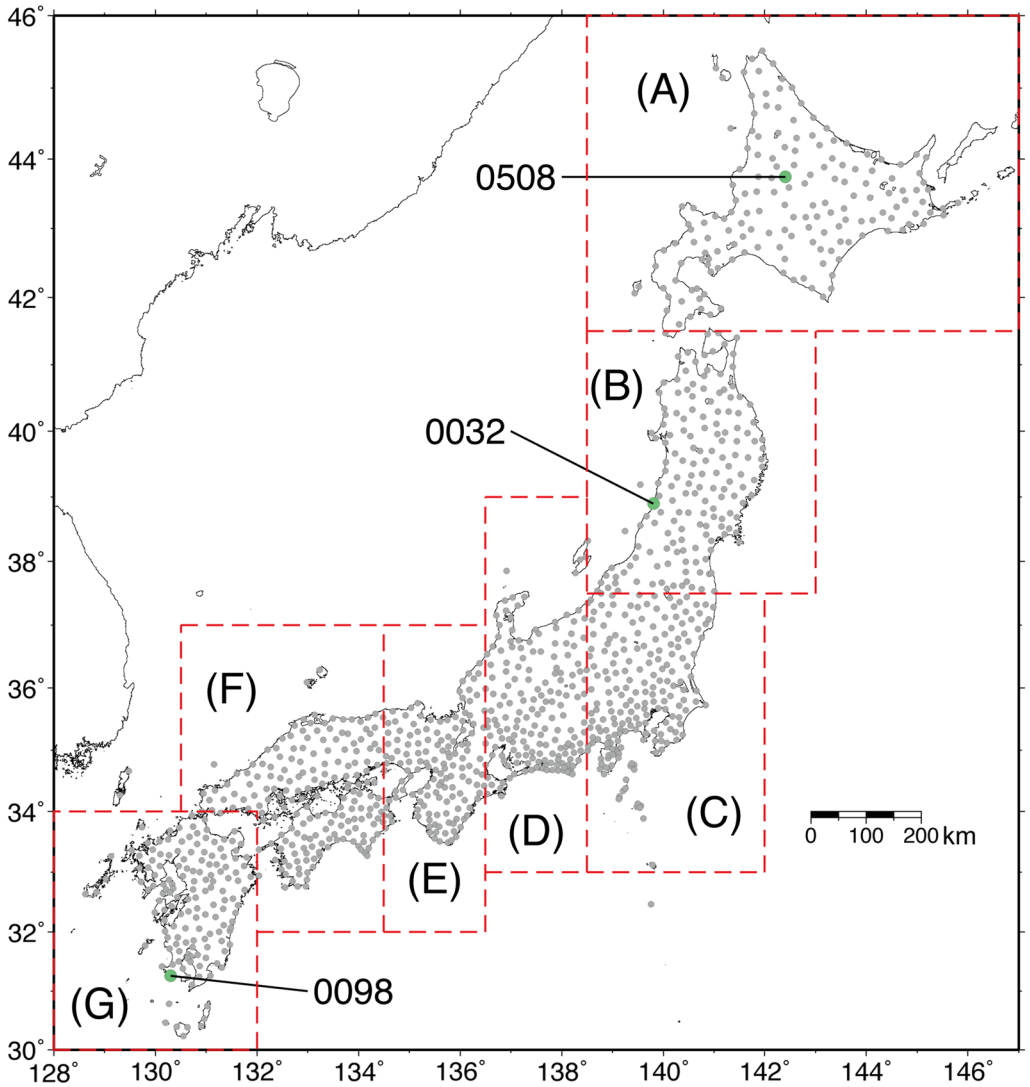

Fig. 1 Map of GNSS stations. *Circles* denote the GEONET stations used in this study. *Solid green circles* indicate the specific station locations used in "Results" and "Discussion" sections. *Dashed red lines* denote the sub-divided regions *A–G* used to assess the regional dependencies of tropospheric parameters

study used only GPS satellites, and Fig. 1 shows the distribution of the GNSS stations used.

To assess the spatial characteristics of the optimum process noise, we analyzed 24-h data recorded across the entire GEONET network from March 10, July 4, and November 22, 2011. The data were processed using GIPSY-OASIS (version 6.3), which provides GNSS data analysis and simulation. We adopted a kinematic PPP strategy (Zumberge et al. 1997) for the coordinate estimation. The reference GPS satellite orbit and clock information were obtained using the Jet Propulsion Laboratory (JPL) final products (known as flinnR). For comparison with the recommended process noise values for the tropospheric parameters suggested by Bar-Sever et al. (1998), we defined an elevation cutoff angle of 7° during data processing. To correct for phase center variation of both the GEONET and GNSS satellites, we applied the absolute antenna phase center variation table provided by the International GNSS Service (IGS). Single-receiver carrier-phase ambiguities were resolved using uncalibrated phase delay (UPD) information provided by the JPL (Bertiger et al. 2010). We corrected the ocean tide loading effect based on the NAO.99b model (Matsumoto et al. 2000) . We estimated the site coordinates every 30 s, assuming a white noise stochastic model with a fixed process noise value (10^{-2} km). In addition, we

estimated ZWD and the tropospheric gradient every 30 s using a random walk stochastic process. Furthermore, we applied a priori information for the zenith tropospheric delay based on the gridded Vienna Mapping Functions 1 (VMF1; Boehm and Schuh 2004) for all of the sites. We computed nominal hydrostatic and wet delays for each site using gridded VMF1 data, which comprises 6-h data with 2.5° × 2.0° spatial resolution. We then applied these calculated nominal tropospheric parameter values as a priori information during kinematic PPP processing.

The stochastic nature of tropospheric parameters such as ZWD and tropospheric gradient affects the changeability of the time series for those unknown parameters. Furthermore, it should also indirectly affect the site coordinate time series. Thus, we assumed that small disturbances in the site coordinate time series should be taken as an optimized result in this study. The three-dimensional root-mean-square (3D-RMS) value is a useful index for assessing the stability of the coordinate time series. However, if 3D-RMS values of the time series are adopted for assessing optimum process noise values, it is difficult to distinguish the effect of process noise value for each coordinate component. Thus, we use the three individual coordinate components for assessing appropriate process noise values. Based on these assumptions, we carried out a grid search for the optimum combination of process noise parameters for the ZWD and tropospheric gradient (hereafter termed TROP and GRAD, respectively), based on the stability of the coordinate time series. We estimated the kinematic site coordinate time series under different combinations of TROP and GRAD parameters for each site. We varied the process noise values for TROP (1×10^{-9} to 1×10^{-5} km $s^{-1/2}$) and GRAD (1×10^{-11} to 1×10^{-7} km $s^{-1/2}$). Each parameter space is divided into 10 combinations, so we estimated the kinematic coordinate time series in 100 combinations. Finally, we calculated the standard deviation (SD) of the time series for each combination of tropospheric process noise parameters for three coordinate components (east–west, north–south, and up–down).

To assess the long-term stability of the optimum tropospheric parameters for a specific site, we analyzed data recorded continuously at stations 0098 and 0032 throughout the year 2010. The locations of these sites are indicated in Fig. 1. We estimated the optimum combination of tropospheric process noise values for each day, using the same procedure as for the spatial characteristic assessment described above.

Results

Characteristics of estimated optimum process noise at specific sites

Figure 2 shows a 1-day kinematic time series example of several combinations of the process noise values for station 0098 with the SD value of each time series. The results clearly show a strong dependency between the TROP and time series in the vertical coordinate component (up–down, UD). The vertical component disturbance clearly increases with increase in the TROP. For example, the calculated SD for low TROP values is 22.7–23.0 mm (Fig. 2a, d). In contrast, the SD result calculated using large values of TROP increases to 42.1–42.7 mm (Fig. 2c, f). Naturally enough, there is strong correlation between the ZWD component and the vertical coordinate component (e.g., Iwabuchi 2003; Penna et al. 2015). The obtained results, therefore, clearly indicate that using an appropriate process noise value has a significant impact on the vertical kinematic time series.

The horizontal coordinate components (e.g., east–west, EW, and north–south, NS) would be expected to correlate with the gradient parameter process noise (e.g., Miyazaki et al. 2003). However, it is difficult to confirm the dependency of the different GRAD process noise values in Fig. 2. Weather conditions on March 10, 2011, were fine in and around station 0098; thus, the atmospheric gradient change should be small. If the atmospheric gradient amount is large, such as during the passage of a weather front, the GRAD process noise value will have a large effect.

Figure 3 shows the SD distributions of the three coordinate components of the kinematic time series for three specific GEONET sites (0032, 0098, and 0508) on March 10, 2011, obtained using a grid-search approach. It is clear that the horizontal components are sensitive to the GRAD process noise. In contrast, the vertical component is sensitive to variations in the TROP parameter. In addition, the optimum combination of both process noise values of each component, which corresponds to the smallest SD value of each time series, varies between the different components. Furthermore, the optimum combination for the same component also varies between the different stations. In contrast, the optimum value of the TROP is relatively constant, ~1×10^{-8} km $s^{-1/2}$, for all three sites (Fig. 3). In the next section, we investigate the possible common optimum combinations of TROP and GRAD values across the entire GEONET network, based on the frequency distributions of the optimum process noise combinations deduced by comparing data from different days.

Characteristics of the estimated optimum process noise combination

Frequency distribution of TROP and GRAD parameter combinations

Figure 4 shows the frequency distribution of optimum TROP and GRAD parameter combinations for each of the east–west (EW), north–south (NS), and up–down (UD) coordinate components, deduced across the entire

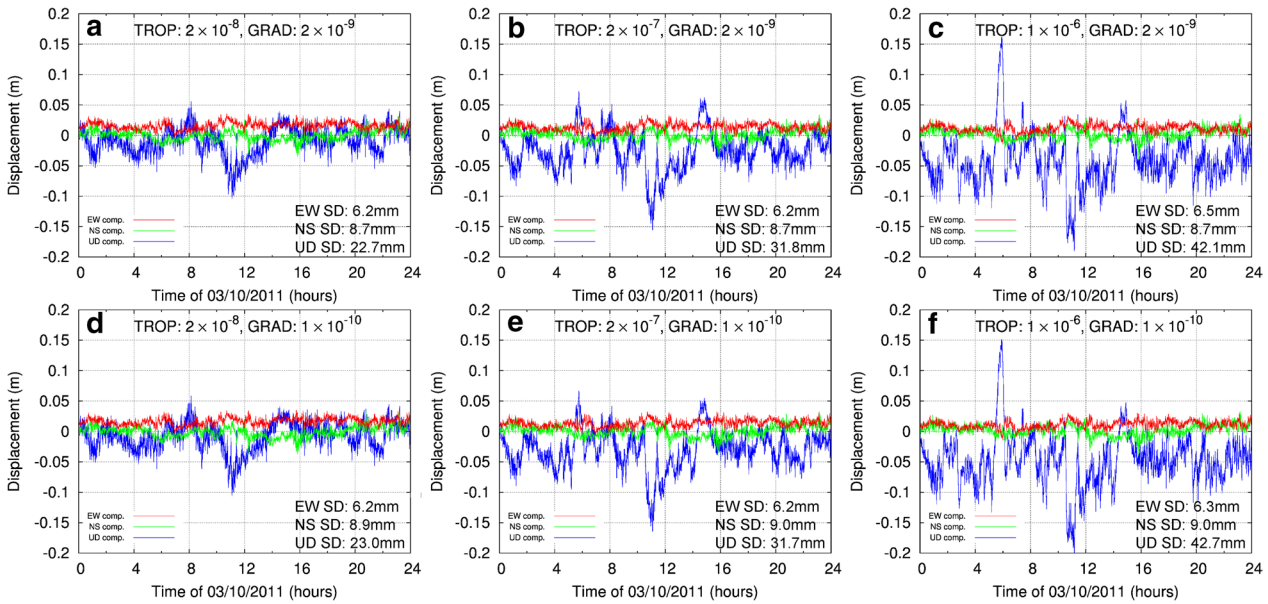

Fig. 2 Kinematic PPP time series example for station 0098 on March 10, 2011, based on the various process noise parameter combinations between zenith wet tropospheric delay and the tropospheric gradient (**a**–**f**). *Red*, *green*, and *blue lines* denote the east–west, north–south, and up–down components, respectively. TROP and GRAD shown at the *top* of each figure represent the process noise value for the zenith wet tropospheric delay and the tropospheric gradient, respectively

GEONET network for March 10, 2011. The colors indicate the ratio of the stations in each combination when the optimum combination value was obtained for each site. The obtained results show that the ratios of the optimum combination value for all of the components are low (<10%). In contrast, the optimum combinations are concentrated in specific regions (indicated by the dashed red squares in Fig. 4) for each component. The sum of the percentages enclosed within the red dashed lines totaled 24.7% for the east–west component, 38.6% for the north–south component, and 70.4% for the vertical component, respectively. The ratio for the vertical component was significantly higher than those of the horizontal components. These results indicate that the optimum combination value for all sites may exist within specific regions in the parameter space.

Additional file 1: Figure S1 and Additional file 2: Figure S2 show the frequency distribution of the TROP and GRAD parameter combinations for each component for July 4 and November 22, 2011, respectively. Weather conditions on July 4 were rainy throughout Japan due to the passage of a cold front. In contrast, November 22 showed clear, fine weather due to high atmospheric pressure across the entire region of Japan. The results in Additional file 1: Figure S1 clearly show the concentration of optimum combinations in a specific region compared with the results from March 10, 2011 (Fig. 4). Furthermore, the maximum value of the GRAD frequency distribution ($\sim 1 \times 10^{-8}$ km $s^{-1/2}$) is larger than that for the March 10 results (Fig. 4, $\sim 2 \times 10^{-9}$ km $s^{-1/2}$). This may reflect the differing weather conditions between the 2 days. This differs from the results for November 22 (Additional file 2: Figure S2), in which the frequency distribution shows slightly complex characteristics; it is clear that the horizontal components did not show a simple distribution, with a comparatively large concentration region in both of the horizontal components (indicated by the dashed red square for EW component and dashed black square for NS component in Additional file 2: Figure S2). The maximum frequency value for the NS component, however, did not locate within this region. In contrast, it is possible to recognize the clear concentration region of the frequency distribution in the vertical component.

Based on these results from the different days, we found that the tendency for concentration of frequency distribution in specific regions is basically a common characteristic despite the twin peaks observed in the horizontal components in the case of November 22 (Additional file 2: Figure S2). Furthermore, the maximum frequency combination differed for each day, which may reflect the differing weather conditions.

Spatial distribution characteristics of the optimum TROP and GRAD parameters

In this section, we show the spatial distribution of the optimum TROP and GRAD parameters for each

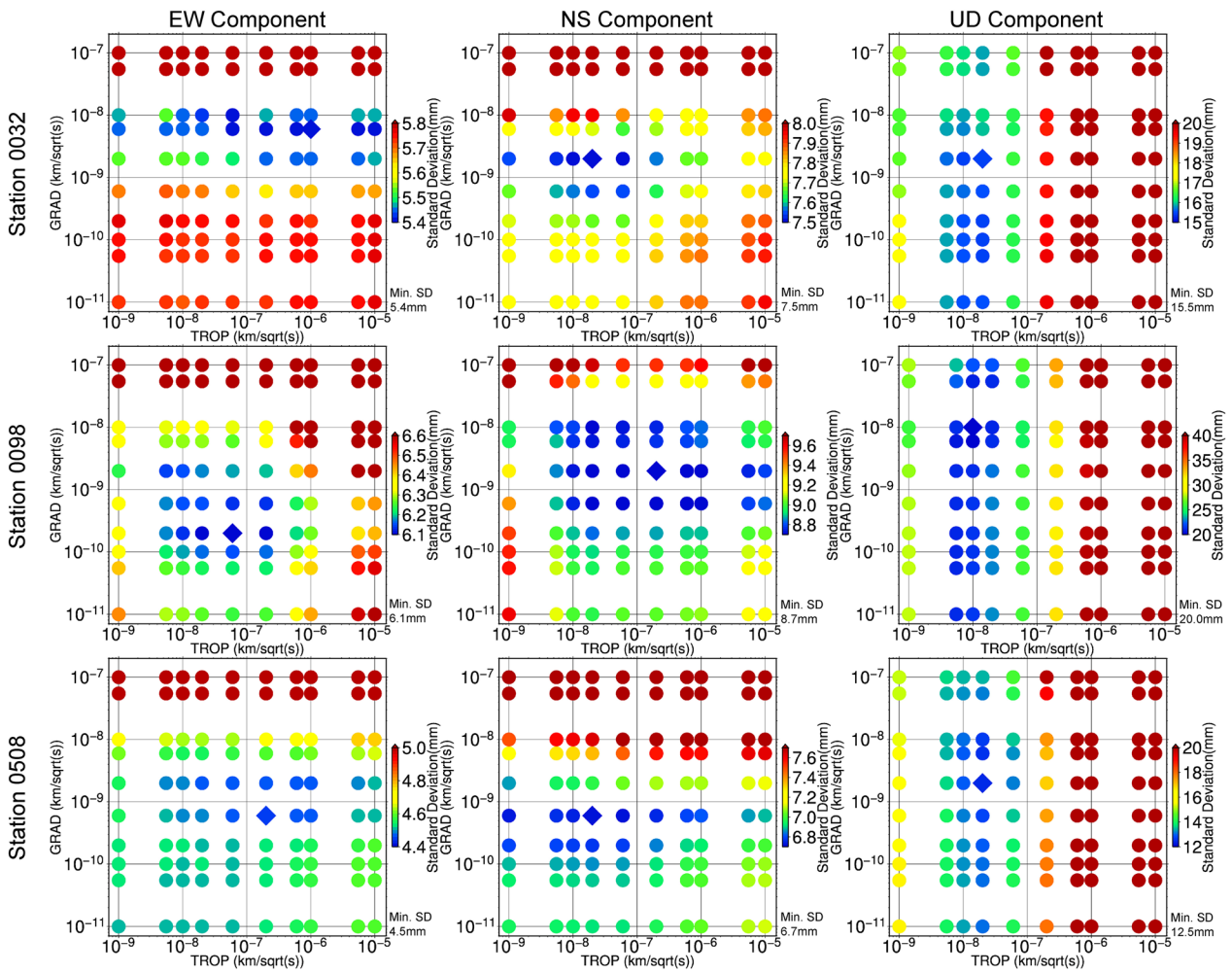

Fig. 3 Distribution of standard deviation (SD) for each station and component on March 10, 2011, based on the various process noise values for zenith wet tropospheric delay (TROP) and tropospheric gradient (GRAD). *Each row* and *column* indicate the specific station and component, respectively. The *diamond* in each figure denotes the minimum SD, which is also shown on the *bottom right* of each figure

calculated day. Firstly, we show the general characteristics, based on the results of the 3 days. Secondly, we show the results for sub-divided region based on the results for March 10, 2011.

Figure 5, Additional file 3: Figure S3, and Additional file 4: Figure S4 show the spatial distribution characteristics of the optimum TROP and GRAD parameters for each of the coordinate components and the calculated SD values for all GEONET stations on March 10, July 4, and November 22, 2011, respectively. We also calculated frequency histograms showing the optimum TROP and GRAD parameters for all GEONET sites (Fig. 6; Additional file 5: Figure S5, Additional file 6: Figure S6).

The distributions of estimated optimum TROP for the vertical component on March 10 and November 22 (Fig. 5(a-3) and Additional file 4: Figure S4(a-3)) clearly show regional characteristics; however, the optimum TROP histogram (Fig. 6e; Additional file 6: Figure S6(e)) for the vertical component shows a steeper distribution than the GRAD parameter (Fig. 6f; Additional file 6: Figure S6(f)). The overall trend indicates that the optimum TROP value for the vertical component in the northern part of Japan is small compared to that in the south (Fig. 5(a-3); Additional file 4: Figure S4(a-3)). However, it is difficult to recognize this trend in the case of July 4, 2011 (Additional file 3: Figure S3(a-3)). The majority (67.7%) of the optimum TROP values were concentrated within a very narrow range around 6×10^{-8} km $s^{-1/2}$ (Additional file 5: Figure S5(e)). Weather conditions on July 4 were rainy throughout Japan, which might affect this characteristic spatial pattern of the optimum TROP distribution.

In comparison with the TROP parameter, the spatial characteristics of the GRAD parameter are less well

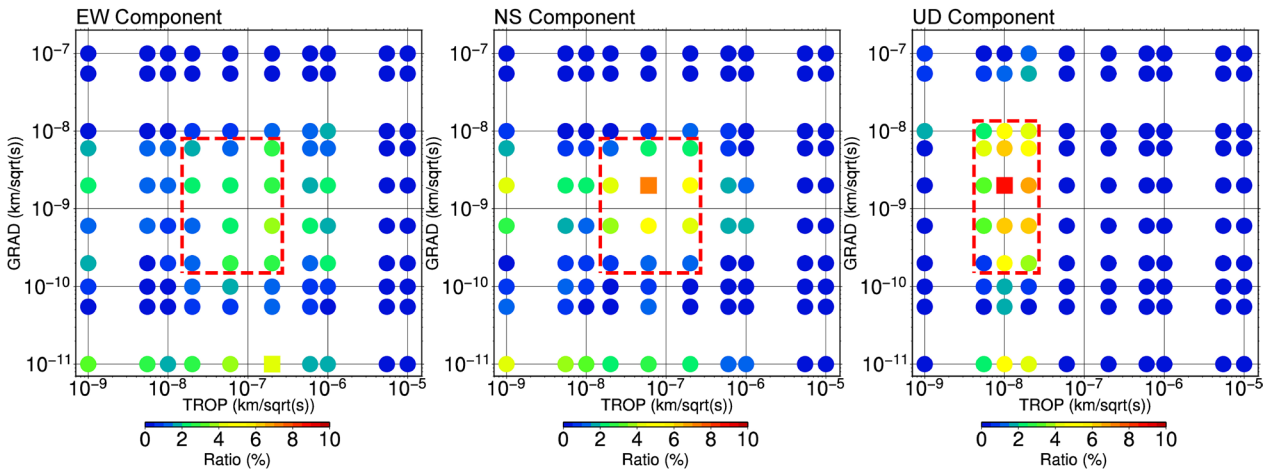

Fig. 4 Frequency distribution of the optimum parameter combinations in TROP and GRAD parameter space, based on data from the entire GEONET network on March 10, 2011. Regions indicated by the *dashed red squares* were used for the common optimum parameter combinations for all components. The *colors* indicate the ratio of the frequency within each parameter combination relative to the number of GEONET sites. The *solid squares* indicated the optimum combination value in each component

defined (Fig. 5; Additional file 3: Figure S3; Additional file 4: Figure S4). The frequency histograms, however, show clear characteristics in each day. For example, in the case of March 10, the frequency histograms of the optimum GRAD parameter for the horizontal components clearly show broader distributions compared to the TROP parameter for the vertical component (Fig. 6). In contrast, the frequency histogram for July 4 clearly shows the steep characteristic for the horizontal components (Additional file 5: Figure S5(b, d)). Weather conditions on July 4 were strongly influenced by the passage of a cold front, such that the obtained results should reflect these weather conditions.

For a more detailed understanding of the spatial characteristics, we show the results for sub-divided regions. In Additional file 7: Figure S7, frequency histograms show the optimum TROP and GRAD for sub-divided regions A–G for the case of March 10 (see also region sub-divisions indicated in Fig. 1) to assess the regional dependency of the TROP and GRAD parameters. Comparison of the calculated histograms for regions (A) and (E) shows that in region (A), the histogram is characterized by a broad distribution with highest frequency optimum TROP value of 1×10^{-8} km $s^{-1/2}$ (Additional file 7: Figure S7). In contrast, the histogram for region (E) shows a much steeper distribution with optimum TROP value of 2×10^{-8} km $s^{-1/2}$ (Additional file 7: Figure S7). These clear differences suggest the optimum process noise might be region-dependent.

The TROP parameter distribution shows a second important characteristic, namely the influence of recording station elevation. Additional file 8: Figure S8 shows the ratio of each optimum TROP parameter within each ellipsoidal GNSS station elevation range for the case of March 10. It is clear that the ratio of low TROP parameter values increased with site elevation. This is a reasonable result because higher elevation is associated with less integration of water vapor. These results suggest that the optimum ZWD process noise parameter might depend on each sub-divided region and the elevation of each site. At this time, the scale of the sub-divided region is several hundred kilometers. Thus, the parameter at least depends on such spatial expansion.

Temporal characteristics of the estimated optimum process noise combination

Figure 7 shows the time series for the estimated optimum process noise values at stations 0098 and 0032 for each coordinate time series component. The gray and red lines denote the daily optimum value and 11-day moving average, respectively.

Interestingly, the optimum TROP time series for the vertical component indicates limited disturbance compared with the horizontal components. Furthermore, the moving average time series obtained at station 0098 shows stability throughout the year (Fig. 7) with small annual pattern. Similarly, at station 0032 the obtained time series is stable despite the minor long-term pattern that developed following day of year (DOY) 100 (Fig. 7). In contrast, the optimum GRAD parameters for the horizontal components show a different tendency. It is clear that the obtained time series did not stabilize during the year, and shows a clear annual pattern in the moving average time series. In the previous

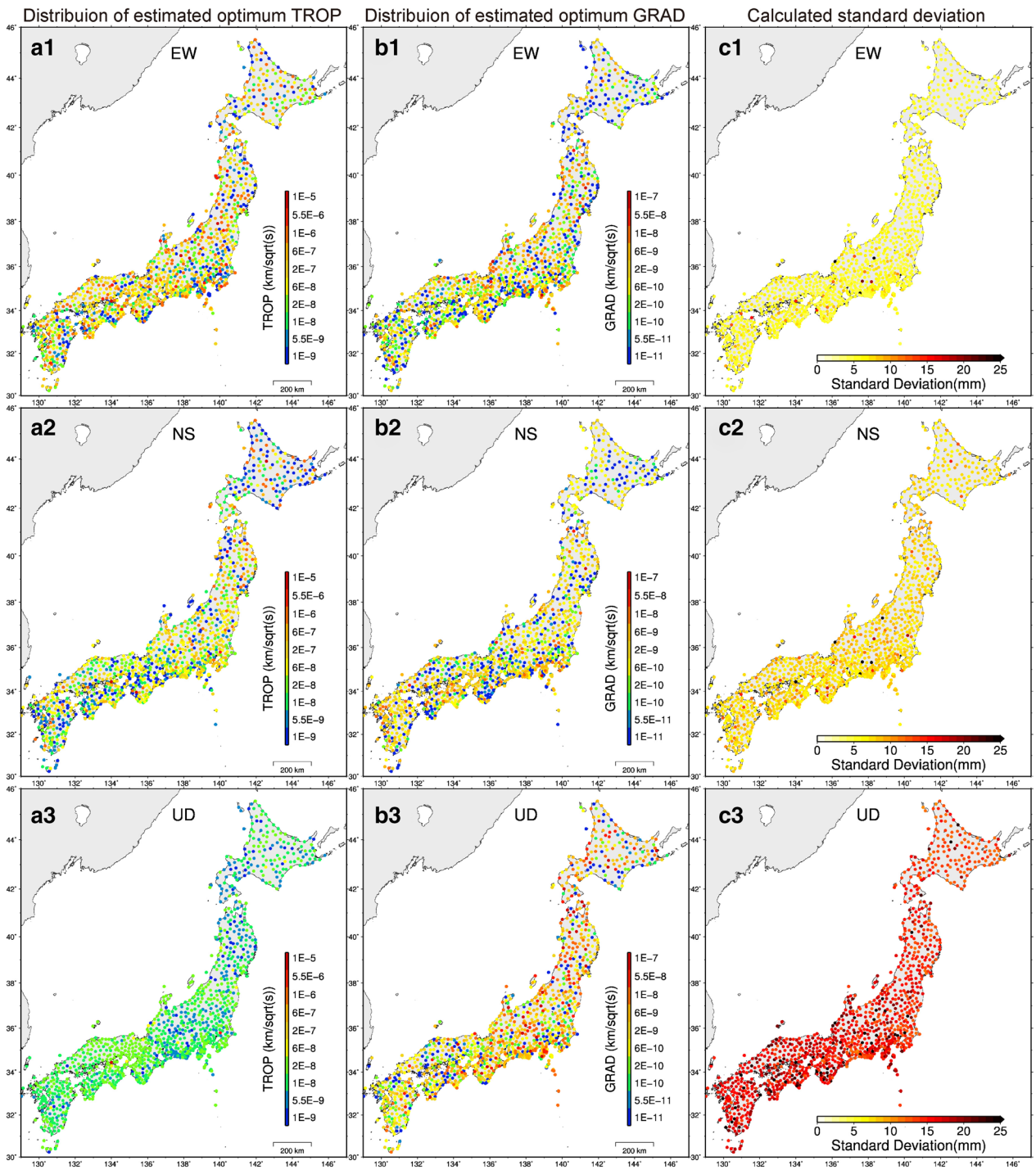

Fig. 5 Distribution of estimated optimum process noise values at each station and standard deviation (SD) based on the optimum process noise value for each component on March 10, 2011. *Each row* shows the specific coordinate component. The *left* (**a1**−**a3**) and *center columns* (**b1**−**b3**) show the estimated optimum process noise values for TROP and GRAD, respectively. The *right column* (**c1**−**c3**) shows the SD distribution based on the estimated optimum process noise values

section, we suggested that the GRAD parameter might not have a significant spatial characteristic within the scale of the GEONET on that specific day. The obtained time series, however, suggests that the optimum GRAD parameter might vary following an annual pattern, despite the relatively large disturbance compared

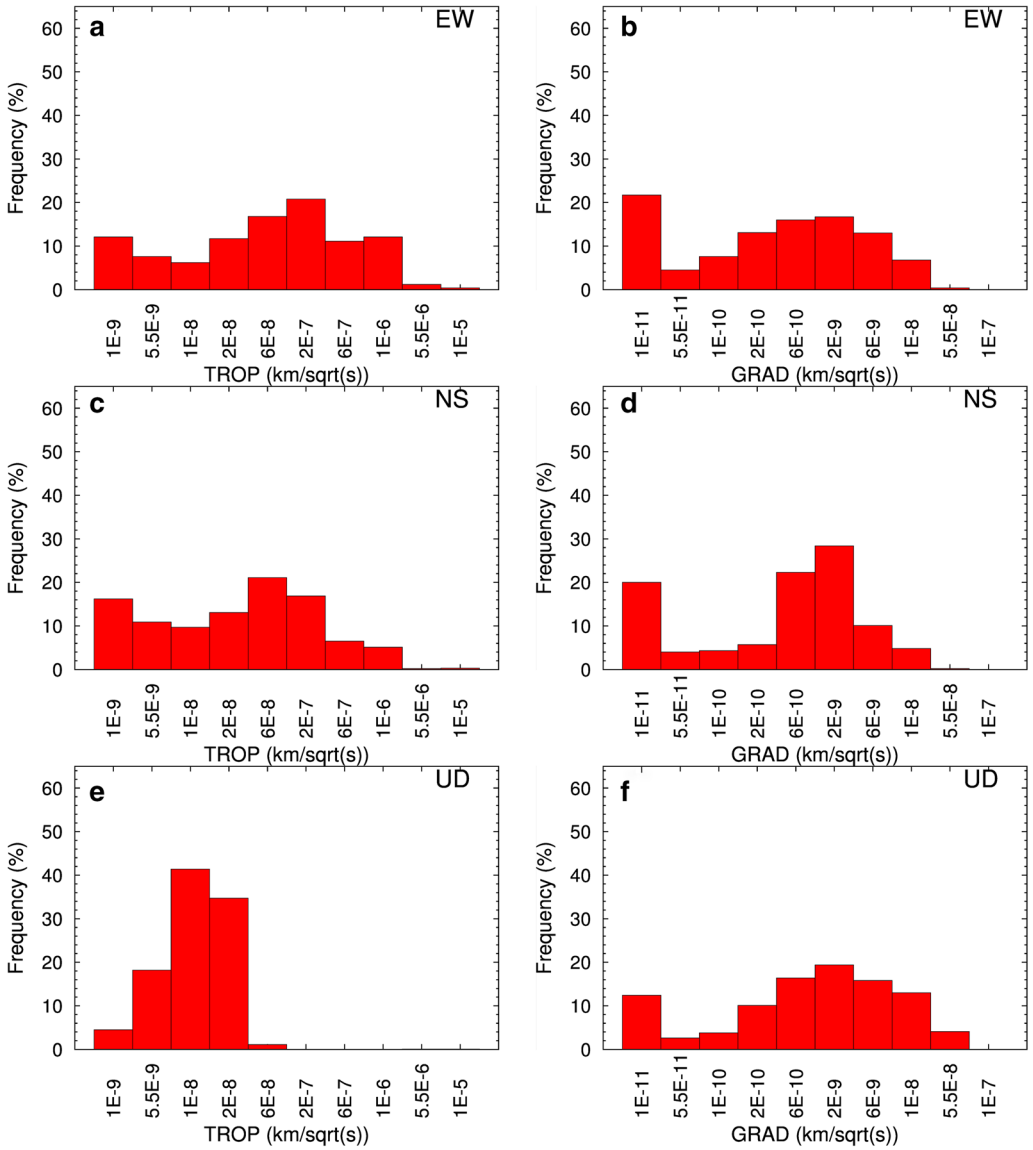

Fig. 6 Histograms showing the estimated optimum process noise value for each component based on data from the entire GEONET network on March 10, 2011. *Left* (**a**, **c**, **e**) and *right columns* (**b**, **d**, **f**) show the TROP and GRAD parameter histograms, respectively

with the optimum TROP parameter for the vertical component.

Yoshida (2010) discussed the spatial annual pattern of tropospheric gradient in Japan deduced from the spatial distribution of the estimated ZWD value at each GEONET site. It was found that the spatial gradient of the ZWD is approximately 130 mm/1000 km and 100 mm/1000 km for summer and winter seasons, respectively. It was also found that the large spatial gradient of ZWD appeared in higher- and lower-latitude regions in the summer and winter seasons, respectively. These results suggest that the annual characteristic of the GRAD parameter at each site might relate to the spatial and temporal characteristics of the GRAD and TROP parameters, even though in the present study the GRAD parameter did not display significant spatial characteristic within 1 day. It is difficult to discuss the relationship between the spatial annual pattern of tropospheric gradient found by Yoshida (2010) and the annual pattern of the optimum GRAD parameter identified in the present study, because our analysis was restricted to only two sites due to limitations on computation time. To investigate the relationship between the two study findings, spatially and temporally dense analysis will be required.

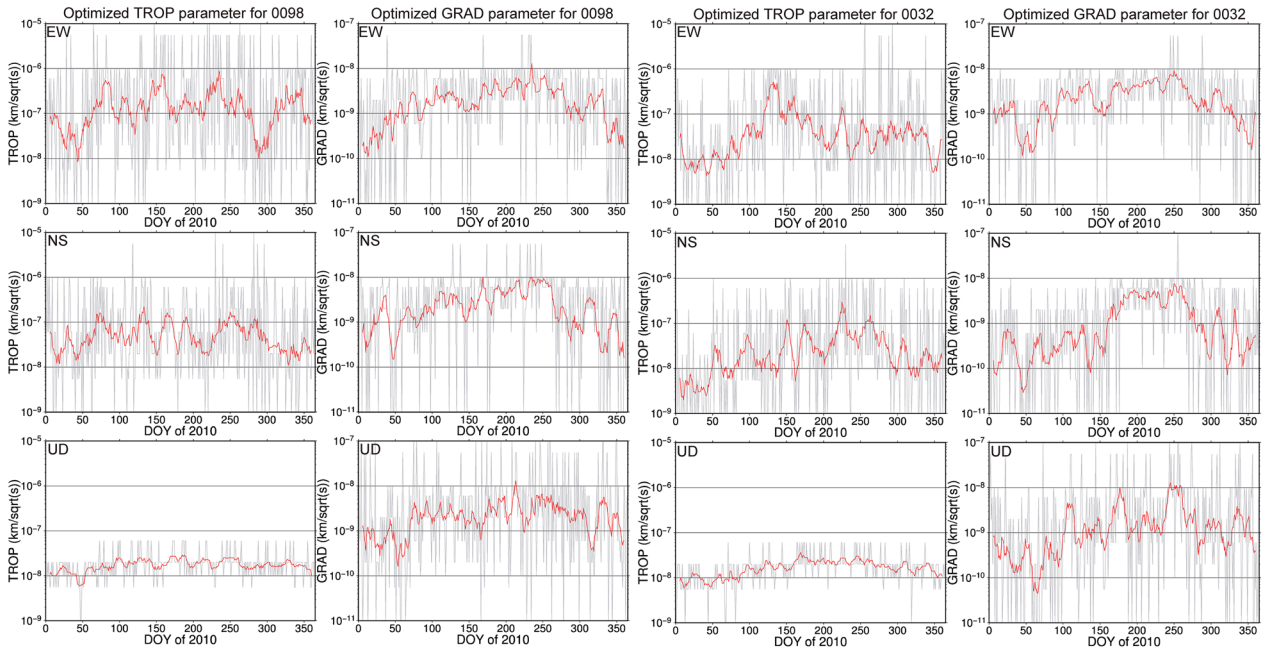

Fig. 7 Estimated optimum process noise value time series at station 0098 (*left side*) and 0032 (*right side*) throughout the year 2010. *Gray* and *red lines* indicate the daily optimum process noise value and 11-day moving average time series, respectively. *Left* and *right columns* for each site indicate the TROP and GRAD parameter for each coordinate component, respectively

Discussion

As summarized in "Introduction" section, determining the appropriate process noise for unknown tropospheric parameters is important for precise analysis of kinematic data. In this section, we discuss the impact of process noise optimization on the kinematic GNSS time series.

Effectiveness of common optimum process noise values for a specific date

In Fig. 4, we presented the frequency distribution of the TROP and GRAD parameter combinations for each coordinate component, deduced from data recorded across the entire GEONET network on March 10, 2011. The obtained results showed that the optimum combinations for each component are concentrated within specific regions of the parameter space (indicated by dashed red squares in Fig. 4). However, the smallest SD combination is different for each component. Thus, we averaged the frequencies of the three components to extract the common optimum process noise combination. The parameter combination comprising a TROP value of 2×10^{-8} km $s^{-1/2}$ and a GRAD value of 2×10^{-9} km $s^{-1/2}$ produced the highest frequency value (~4.3%). Thus, we adopted these process noise values as the "common" optimum parameters for this specific date.

Using these estimated common optimum process noise values on March 10 gives improved SD for all sites when compared with the values recommended by Bar-Sever et al. (1998), except for three outlier sites (0055, 0151, and 0676) that have very large SD (Fig. 8). The large outlier values at these three sites might be caused by the multipath, because similar large disturbance also appeared the day before March 10, 2011. It is clear that SD improved for the majority of stations, despite the observation that the optimum parameters should depend on each sub-divided region and station elevation (Additional file 7: Figure S7; Additional file 8: Figures S8). The averaged improvements in SD for all GEONET sites except the three outliers mentioned above are 6.6% (SD = 7.6–7.1 mm), 6.3% (SD = 10.1–9.5 mm), and 22.4% (SD = 31.2–24.2 mm) for the east–west, north–south, and vertical components, respectively. We also found concentrations of optimum process noise combinations within specific parameter space during the other days (Additional file 1: Figure S1; Additional file 2: Figure S2). For example, the averaged improvements in SD for all GEONET sites for July 4 are 0.7% (SD = 12.8–12.7 mm), 1.9% (SD = 16.0–15.7 mm), and −0.3% (SD = 37.8–37.9 mm) for the east–west, north–south, and vertical components, respectively. In the east–west and vertical component, the estimated optimum parameter combination is almost the same as the results obtained using the recommended values. For the case of November 22, as mentioned in

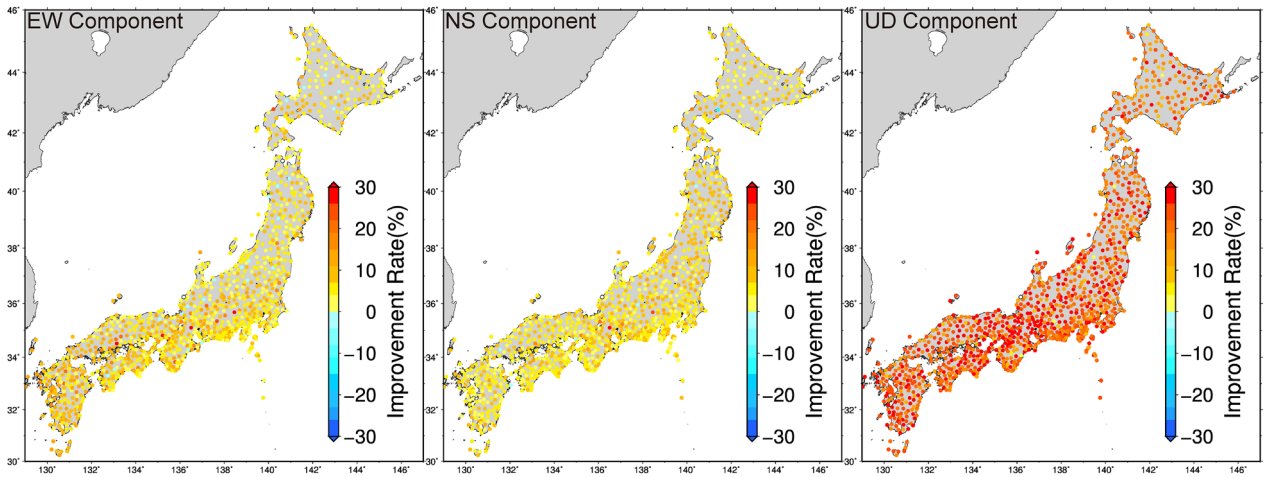

Fig. 8 Spatial distribution of improvements in coordinate time series for each coordinate component on March 10, 2011, based on the estimated "common" optimum process noise values. The *color of each circle* indicates the improvement rate at each station. Warm and cold colors denote positive and negative changes, respectively, at each station. Three outlier sites, which show very large SD, are indicated with *open circles*

previously, we found twin peaks in the frequency distribution, especially in the horizontal components. Thus, we calculated the common optimum process noise values for each peak region based on the three components. First, common optimum process noise values on November 22 are a TROP value of 1×10^{-8} km $s^{-1/2}$ and a GRAD value of 6×10^{-10} km $s^{-1/2}$. The averaged improvements in SD for all GEONET sites are 16.8% (SD = 10.1–8.4 mm), 15.6% (SD = 13.4–11.3 mm), and 32.3% (SD = 35.9–24.3 mm) for the east–west, north–south, and vertical components, respectively. The second common optimum process noise values are a TROP value of 5.5×10^{-9} km $s^{-1/2}$ and a GRAD value of 1×10^{-11} km $s^{-1/2}$. The averaged improvements in SD for all GEONET sites are 16.8% (SD = 10.1–8.4 mm), 15.6% (SD = 13.4–11.3 mm), and 29.0% (SD = 35.9–25.5 mm) for the east–west, north–south, and vertical components, respectively. Both of the results clearly show the improvements in SD. These results suggest that the assumption of "common" optimum process noise is useful for improving the coordinate time series. The percentage improvement in the vertical component is significantly greater than for the horizontal components. This result further suggests that the treatment of the process noise for ZWD estimation is sensitive to the vertical component of the kinematic PPP time series.

Practical application of optimum process noise values in kinematic analysis

In this study, we assessed the spatial and temporal characteristics of process noise values for unknown tropospheric parameters. The findings clearly indicate the importance of optimizing the process noise. However, using a daily grid-search approach to determine the optimum process noise combination for each site may be unfeasible, due to excessive computational demands. In the previous section, we described the effectiveness of using a "common" process noise value for each specific day across the GEONET network; however, this approach also requires considerable computational resources. Thus, for practical use, it is important to develop a method of determining these "optimum" values within realistic computation times, which is beyond the scope of the present study. These approaches should be useful for both GEONET and other GNSS networks. Once the optimum process noise parameters are experimentally and/or theoretically determined for each station or each network, the results will contribute significantly to the understanding of short-timescale crustal deformation with periods of less than 1 day, using kinematic GNSS analysis.

Conclusions

In this study, we assessed the spatial and temporal characteristics of process noise values for unknown tropospheric parameters in kinematic analysis of GNSS data from the GEONET network, Japan. We used a grid-search approach to extract optimum process noise values for each site on 3 days during 2011.

Based on the values determined for each site, we investigated the spatial and temporal characteristics of the process noise parameters. The spatial distribution of the optimum process noise value for the zenith wet tropospheric parameter with vertical site coordinate clearly

shows regional characteristics and is also dependent on station elevation. In contrast, the optimum process noise for the tropospheric gradient might not have significant spatial distribution characteristics within the scale of the GEONET network on that specific day. The temporal characteristics of the optimum process noise parameters for each site coordinate component at specific sites showed a clear annual pattern in the tropospheric gradient parameter of the horizontal components.

Finally, we assessed the impact of process noise optimization for the kinematic GNSS site coordinate time series. For the calculation, we assumed the "common" optimum process noise values for a specific day (March 10, 2011) across the entire GEONET network. These gave improved site coordinate time series (i.e., smaller standard deviation) compared with the recommended values proposed by Bar-Sever et al. (1998), with the exception of some outlier sites. These results suggest that the use of appropriate process noise values is important for analyzing kinematic GNSS time series.

Additional files

Additional file 1: Figure S1. Frequency distribution of the optimum parameter combinations in TROP and GRAD parameter space, based on data from the entire GEONET network on July 4, 2011. Regions indicated by the *dashed red squares* denote the high-frequency region in each component. The *colors* indicate the ratio of the frequency within each combination of the parameters relative to the number of GEONET sites. The *solid squares* indicated the optimum combination value in each component.

Additional file 2: Figure S2. Frequency distribution of the optimum parameter combinations in TROP and GRAD parameter space, based on data from the entire GEONET network on November 22, 2011. Regions indicated by the *dashed red squares* denote the high-frequency region in each component. *Dashed black squares* denote the second peak of the high-frequency distribution of the optimum parameter combinations. The colors indicate the ratio of the frequency within each combination of the parameters relative to the number of GEONET sites. The *solid squares* indicated the optimum combination value in each component.

Additional file 3: Figure S3. Distribution of estimated optimum process noise values at each station and standard deviation (SD) based on the optimum process noise value for each component on July 4, 2011. *Each row* shows the specific coordinate component. The left and center columns show the estimated optimum process noise values for TROP and GRAD, respectively. The right column shows the SD distribution based on the estimated optimum process noise values.

Additional file 4: Figure S4. Distribution of estimated optimum process noise values at each station and standard deviation (SD) based on the optimum process noise value for each component on November 22, 2011. *Each row* shows the specific coordinate component. The *left* and *center columns* show the estimated optimum process noise values for TROP and GRAD, respectively. The *right column* shows the SD distribution based on the estimated optimum process noise values.

Additional file 5: Figure S5. Histograms showing the estimated optimum process noise value for each component based on data from the entire GEONET network on July 4, 2011. *Left* and *right columns* show the TROP and GRAD parameter histograms, respectively.

Additional file 6: Figure S6. Histograms showing the estimated optimum process noise value for each component based on data from the entire GEONET network on November 22, 2011. *Left* and *right columns* show the TROP and GRAD parameter histograms, respectively.

Additional file 7: Figure S7. Histograms showing estimated optimum process noise values for each component in sub-regions A–G (see Fig. 1) on March 10, 2011. *Left* and *right columns* show the TROP and GRAD parameter histograms, respectively, in each region.

Additional file 8: Figure S8. Histogram showing estimated optimum zenith wet tropospheric delay (TROP) parameter in each ellipsoidal height range for the entire GEONET network on March 10, 2011. The *colors* indicate the TROP parameter value.

Acknowledgements
We are grateful to the GSI for providing the GEONET GNSS data and to the Jet Propulsion Laboratory for providing high-quality precise GPS ephemerides and clock information. We would like to thank three anonymous reviewers and the associate editors for their many constructive comments on an earlier draft of the manuscript. This study was partly supported by the Ministry of Education, Culture, Sports, Science, and Technology (MEXT) of Japan, under its Earthquake and Volcano Hazards Observation and Research Program. This work was also supported by the Japan Society for the Promotion of Science (JSPS) under KAKENHI Grant Number 15H03713 and 15K13556. We would like to thank Editage (www.editage.jp) for English language editing.

Received: 7 March 2016 Accepted: 26 November 2016
Published online: 08 December 2016

References

Bar-Sever YE, Kroger PM, Borjesson JA (1998) Estimating horizontal gradients of tropospheric path delay with a single GPS receiver. J Geophys Res 103(B3):5019–5035. doi:10.1029/97JB03534

Bertiger W, Desai SD, Haines B, Harvey N, Moore AW, Owen S, Weiss JP (2010) Single receiver phase ambiguity resolution with GPS data. J Geod 84:327–337. doi:10.1007/s00190-010-0371-9

Bilich A, Cassidy JF, Larson KM (2008) GPS seismology: application to the 2002 M_w 7.9 Denali Fault Earthquake. Bull Seismol Soc Am 98(2):593–606. doi:10.1785/0120070096

Boehm J, Schuh H (2004) Vienna mapping functions in VLBI analyses. Geophys Res Lett 31(1):L01603. doi:10.1029/2003GL018984

Davis JL, Herring TA, Shapiro II, Rogers AEE, Elgered G (1985) Geodesy by radio interferometry: effects of atmospheric modeling errors on estimates of baseline length. Radio Sci 20:1593–1607

Delouis B, Nocquet J-M, Vallée M (2010) Slip distribution of the February 27, 2010 Mw = 8.8 Maule Earthquake, central Chile, from static and high-rate GPS, InSAR, and broadband teleseismic data. Geophys Res Lett 37(17):L17305. doi:10.1029/2010GL043899

Genrich JF, Bock Y (2006) Instantaneous geodetic positioning with 10–50 Hz GPS measurements: noise characteristics and implications for monitoring networks. J Geophys Res 111(B3):1–12. doi:10.1029/2005JB003617

Iwabuchi T (2003) An impact of estimating tropospheric delay gradients on tropospheric delay estimations in the summer using the Japanese nationwide GPS array. J Geophys Res 108(D10):4315. doi:10.1029/2000JB000113

Kawamoto S, Hiyama Y, Ohta Y, Nishimura T (2016) First result from the GEONET real-time analysis system (REGARD): the case of the 2016 Kumamoto Earthquakes. Earth Planets Space 68:190. doi:10.1186/s40623-016-0564-4

Larson KM, Miyazaki S (2008) Resolving static offsets from high-rate GPS data: the 2003 Tokachi-oki earthquake. Earth Planets Space 60(8):801–808. doi:10.1186/BF03352831

Larson KM, Bodin P, Gomberg J (2003) Using 1-Hz GPS data to measure deformations caused by the Denali Fault Earthquake. Science 300(5624):1421–1424. doi:10.1126/science.1084531

Lichten SM, Border JS (1987) Strategies for high-precision Global Positioning System orbit determination. J Geophys Res 92(B12):12751–12762. doi:10.1029/JB092iB12p12751

MacMillan DS (1995) Atmospheric gradients from very long baseline interferometry observations. Geophys Res Lett 22(9):1041–1044. doi:10.1029/95GL00887

Matsumoto K, Takanezawa T, Ooe M (2000) Ocean tide models developed by assimilating TOPEX/POSEIDON altimeter data into hydrodynamical model: a global model and a regional model around Japan. J Oceanogr 56:567–581. doi:10.1023/A:1011157212596

Melgar D, Bock Y (2013) Near-field tsunami models with rapid earthquake source inversions from land and ocean based observations: the potential for forecast and warning. J Geophys Res 118:5939–5955. doi:10.1002/2013JB010506

Melgar D, Crowell BW, Bock Y, Haase JS (2013) Rapid modeling of the 2011 Mw 9.0 Tohoku-oki earthquake with seismogeodesy. Geophys Res Lett 40:2963–2968. doi:10.1002/grl.50590

Melgar D, Geng J, Crowell BW, Haase JS, Bock Y, Hammond WC, Allen RM (2015) Seismogeodesy of the 2014 Mw 6.1 Napa earthquake, California: rapid response and modeling of fast rupture on a dipping strike-slip fault. J Geophys Res: Solid Earth 120:5013–5033. doi:10.1002/2015JB011921

Miyazaki S, Larson KM (2008) Coseismic and early postseismic slip for the 2003 Tokachi-oki earthquake sequence inferred from GPS data. Geophys Res Lett 35(4):1–5. doi:10.1029/2007GL032309

Miyazaki S, Iwabuchi T, Heki K, Naito I (2003) An impact of estimating tropospheric delay gradients on tropospheric delay estimations in the summer using the Japanese nationwide GPS array. J Geophys Res 108(B7):2335. doi:10.1029/2000JB000113

Miyazaki S, Larson K, Choi K, Hikima K, Kokoetsu K, Bodin P, Hasse J, Emore G, Yamagiwa A (2004) Modeling the rupture process of the 2003 September 25 Tokachi-Oki (Hokkaido) earthquake using 1-Hz GPS data. Geophys Res Lett 31(21):L21603. doi:10.1029/2004GL021457

Ohta Y, Meilano I, Sagiya T, Kimata F, Hirahara K (2006) Large surface wave of the 2004 Sumatra-Andaman earthquake captured by the very long baseline kinematic analysis of 1-Hz GPS data. Earth Planets Space 58(2):153–157. doi:10.1186/BF03353372

Ohta Y, Kobayashi T, Tsushima H, Miura S, Hino R, Takasu T, Fujimoto H, Iinuma T, Tachibana K, Demachi T, Sato T, Ohzono M, Umino N (2012) Quasi real-time fault model estimation for near-field tsunami forecasting based on RTK-GPS analysis: application to the 2011 Tohoku-Oki earthquake (Mw 9.0). J Geophys Res 117(B2):B02311. doi:10.1029/2011JB008750

Ohta Y, Kobayashi T, Hino R, Demachi T, Miura S (2015) Rapid coseismic fault determination of consecutive large interplate earthquakes: the 2011 Tohoku-Oki sequence. International Association of Geodesy Symposia. doi:10.1007/1345_2015_109

Penna NT, Clarke PJ, Bos MS, Baker TF (2015) Ocean tide loading displacements in western Europe: 1. Validation of kinematic GPS estimates. J Geophys Res 120(9):6523–6539. doi:10.1002/2015JB011882

Webb SR, Penna NT, Clarke PJ, Webster S, Martin I, Bennitt GV (2016) Kinematic GNSS estimation of zenith wet delay over a range of altitudes. J Atmos Ocean Technol 33(1):3–15. doi:10.1175/JTECH-D-14-00111.1

Yokota Y, Koketsu K, Hikima K, Miyazaki S (2009) Ability of 1-Hz GPS data to infer the source process of a medium-sized earthquake: the case of the 2008 Iwate-Miyagi Nairiku, Japan, earthquake. Geophys Res Lett 36(12):L12301. doi:10.1029/2009GL037799

Yoshida K (2010) GPS Climatology: Climatological signals from long term behaviors of atmospheric zenith delays and their gradients from the Japanese dense GPS array. Master's dissertation, Hokkaido University, Japan

Zumberge J, Heflin M, Jefferson D (1997) Precise point positioning for the efficient and robust analysis of GPS data from large networks. J Geophys Res 102(B3):5005–5017. doi:10.1029/96JB03860